

UDK: 549.73; 53.086

## Effects of Heat Treatment on Characteristics of Zn Substituted Co/Mn Ferrite Nanoparticles

Nasrallah M. Deraz<sup>\*)</sup>

Physical Chemistry Department, National Research Centre, 33 El Bohouth St. (El-Tahrir St. former), Dokki, Giza, P.O.12622, Egypt

---

### Abstract:

*Glycine assisted self-combustion method resulted in fabrication of cobalt-manganese ferrite substituted by zinc (Zn) element. The as-synthesized Zn substituted Co- Mn ferrite was subjected to heat treatment at 600 °C and 800 °C for 2h. Effects of heat treatment on the structural, morphological, surface and magnetic properties of ZnCoMn ferrite were studied. These properties were characterized by using various techniques including TGA-DTGA, FTIR, XRD, SEM, EDX, TEM and VSM. The results showed that the used preparation route led to the formation of nano crystalline  $Zn_{0.2}Co_{0.4}Mn_{0.4}Fe_2O_4$  particle with cubic spinel type structure. The crystallinity of this ferrite increases as the heat treatment increases. However, the preparation method resulted to the creation of spongy, fluffy, foamy and fragile material with cubic type structure with some agglomerations. Increasing the calcination temperature from 600 °C to 800 °C, led to a decrease in the surface area (39.4 %) of the as-synthesized ferrite. This treatment causes an increase in the magnetization(40.3 %) of this ferrite. The heat treatment that led to various changes in the different properties of the manufactured ferrite was discussed.*

**Keywords:** XRD; FTIR; SEM; ZnCoMn ferrite; Magnetization.

---

### 1. Introduction

The solid state reaction between ferric oxide and oxide of any other elements resulted in the formation of elements based ferrites. These ferrites can be classified simple and mixed ferrites owing different properties. Tuning of this reaction between different constituents of ferrites depends on the contact surface area between these components and their mobility. Stimulation of the mobility of the reacting oxides taking the part formation of ferrite depends on different factors. These factors were multiplied, gradual, and even differed in their impact on the formation of different ferrites. Among these factors are, the doping, temperature, precursors, preparation method and substitution process.

Ferrites have a great position among the advanced materials with future applications because of their unconventional properties, especially when produced in the nano-size. Since one of the requirements of the modern era is the necessity of the existence of communications, home appliances and electronic industries, the ferrites had the greatest and great role in all of the above.

As one of the most important concerns of Deraz Group is the preparation and characterization of various ferrites in simple, inexpensive and environmentally friendly ways, manganese ferrites and their derivatives were among these interests and studies [1]. In fact,

---

<sup>\*)</sup> Corresponding author: amn341@yahoo.com

manganese ferrite ( $\text{MnFe}_2\text{O}_4$ ) has inverse spinel structure because the  $\text{Mn}^{2+}$  ions occupy only the tetrahedral (A) sites, while the  $\text{Fe}^{3+}$  ions populate the octahedral (B) sites [1, 2]. In addition, 80% of Mn ions occupy A-site, which is surrounded by four  $\text{O}^{2-}$  ions, and the left 20% of Mn ions occupy B-site, which is surrounded by six  $\text{O}^{2-}$  ions [2, 3]. In other words,  $\text{Mn}^{2+}$  ions are randomly distributed between A and B sites [3, 4]. Moreover,  $\text{MnFe}_2\text{O}_4$  is a soft ferrite characterized by high magnetic permeability and low hysteresis losses [1]. A progressive change in the different properties of  $\text{MnFe}_2\text{O}_4$  nano particles was studied with the substitution by  $\text{Zn}^{2+}$  ions [5]. When the  $\text{Mn}^{2+}$  ions are substituted by  $\text{Zn}^{2+}$  ions,  $\text{Zn}^{2+}$  ions are expected to occupy A-site, while  $\text{Mn}^{2+}$  ions are randomly distributed between A- and B-sites [1, 5]. On the other hand, the combustion route can be used in preparation of nano sized zinc-substituted cobalt ferrite powders with different content of ZnO. Because the substitution process had a strong and noticeable effect in changing the properties of simple ferrites, the studies of groups were directed towards mixed and/or substituted ferrites, including  $\text{Co}_{1-x}\text{Zn}_x\text{Fe}_2\text{O}_4$  nano particles ( $x = 0, 0.25, 0.5, 0.75$  and 1) [7]. In the spinel  $\text{CoZn}$  ferrites, the value of saturation magnetization ( $M_s$ ) was varied by changing the value of  $x$ . The maximum value of  $M_s$  was observed in case of partial substitution with  $\text{Co}_{0.25}\text{Zn}_{0.75}\text{Fe}_2\text{O}_4$  crystallites. This augmentation in the saturation magnetization speculated that this method is suitable for preparing high-quality nano-sized magnetic ferrites for practical applications [7].

There are many ways to obtain different ferrites, including co-precipitation, sol gel, hydrothermal and micro-emulsion [11, 12]. Glycine assisted combustion method is one of the simple, inexpensive and quick ways to prepare different ferrites [1, 5, 7-10]. In our previous study of  $\text{Zn}_{0.2}\text{Co}_{0.4}\text{Mn}_{0.4}\text{Fe}_2\text{O}_4$  system, we found that the combustion method based on glycine as fuel led to obtaining a single phase with specified properties [13]. Therefore, it was directed to study the effect of different temperatures on various properties of this system prepared in the same previous method. The objective of this study was to prepare mixed ferrites with different ratios of Zn, Co, and Mn elements by using glycine assisted combustion route followed by heating at 600 °C and 800 °C for 2h.

This work aims to prepare of Zn substituted Co/Mn ferrite using glycine mediated combustion method followed by heat treatment at 600 °C and 800 °C for 2h. Characterization of the as prepared ferrites was achieved using different techniques such as TGA-DTGA, XRD and FTIR. Surface and magnetic properties of the as synthesized ferrites were determined. Finally, the effects of the heat treatment at 600 and 800 °C on the structural, morphological, surface and magnetic properties of Zn substituted Co/Mn ferrite were discussed.

## 2. Materials and Experimental Procedures

### 2.1. Materials

All the reagents (some transition metals nitrates) were of analytical grade without any purification, ferric nitrate,  $\text{Fe}(\text{NO}_3)_3 \cdot 9\text{H}_2\text{O}$ , manganese nitrate,  $\text{Mn}(\text{NO}_3)_2 \cdot 4\text{H}_2\text{O}$ , cobalt nitrate  $\text{Co}(\text{NO}_3)_2 \cdot 6\text{H}_2\text{O}$  and Zinc nitrate,  $\text{Zn}(\text{NO}_3)_2 \cdot 6\text{H}_2\text{O}$ , and glycine,  $\text{NH}_2\text{CH}_2\text{COOH}$ .

### 2.2. Preparation method

In this study, the investigated ferrites were prepared using the previously used glycine assisted combustion method [13]. Two samples of mixed quarterly transition metal ferrite (MQTMF) solid were prepared by adding a certain amount of glycine to calculated amounts of mixture of Zn, Co and Mn nitrates with strong stirring at room temperature to manufacture a well-dissolved solution as sol. Then, the sol was converted to gel by heating on a hot plate at 80 °C with vigorous stirring. When a vessel temperature was reached to 300 °C for 15 min., a lot of foams resulted and spark observed at one corner of vessel. This spark

spread through the mass, yielding a voluminous and fluffy product. The as-prepared products were crushed into powders using a mortar and pestle. Finally, the obtained powders were calcined at 600 °C and 800 °C for 2h, and labeled with symbols as S1 and S2, respectively. In this study, mass ratio of the glycine: Zn nitrate : Co nitrate : Mn nitrate: Fe nitrate were 3: 0.59495: 1.164136: 1.00404: 8.08 g, respectively.

### 2.3. Techniques for determination of the studied systems properities

A thermal analyzer, the Nietzsche 449 Jupiter design (Weimar, Döbereiner, Germany) has been used to acquire simultaneous thermogravimetry - differential thermogravimetry (TGA—DTGA) measurements. The investigations were performed under a nitrogen gas atmosphere in a temperature range of 25–1000 °C at a gas flow rate of 40 mL min<sup>-1</sup>. The rate of heating of the test sample was 10 °C min<sup>-1</sup>.

X-ray diffraction technology (Germany) based on A BRUKER D8 advance diffractometer was used to characterize various mixed solids. The illustrated patterns were obtained using Cu *Ka* radiation at 40 kV, 40 mA with a 2° min<sup>-1</sup> scanning speed. X-ray diffraction line broadening and Scherrer equation calculations resulted in determination of the crystallite size of Zn substituted Co-Mn ferrites studied [16].

$$d = \frac{B\lambda}{\beta \cos \theta} \quad (1)$$

where *d*, *B*, *λ*, *β* and *θ* are the average crystallite size of the crystalline phase, Scherrer constant, wavelength of the X-ray beam, the full-width half maximum (FWHM) of diffraction and the Bragg's angle.

Determination of the Fourier-transmission infrared spectrum (FTIR) of different ferrites studied can be achieved by using Perkin-Elmer Spectrophotometer (type 1430). The FTIR spectra were determined at room temperature in the range between 4000 and 400 cm<sup>-1</sup>. 2 mg of each solid specimen was combined with 0.2 g of IR-grade KBr which has been vacuum-dried. A vibratory ball mill was used to ground the combination for 3 min. The product was placed in a steel die 13 mm in diameter, and under 12 tons of pressure to scatter it. The identical disks were used to fill the holder of the double-grating FTIR spectrophotometer.

JEOL JAX-840A and JEOL Model 1230 (JEOL, Tokyo, Japan) enabled us to recode scanning electron microscope (SEM), *energy-dispersive X-ray spectroscopy* (EDS) and transmittance electron micrograph (TEM). In order to disperse individual particles over mount setup and Copper grids, the specimens were dispersed in ethanol and then treated ultrasonically for a few minutes.

Using the Brunauer-Emmett-Teller method and surface area analyzers from Micrometrics' Gemini VII 2390 V1.03 series resulted to a determination of the surface area (*S*<sub>BET</sub>), total pore volume (*V*<sub>P</sub>), and mean pore radius (*r̄*) for the as-prepared materials. Before the measurements, each sample was out-gassed for 2 hours at 200 °C and a lower pressure of 10<sup>-5</sup> Torr. The magnetic properties of the as-synthesized ferrites were determined by using a vibrating sample magnetometer (VSM; 9600-1 LDJ, USA) with a maximum applied field of 20 kG.

## 3. Results

### 3.1. Thermal analysis

TGA/DTGA curves of manufactured MQTMF sample are shown in Fig. 1. Over the temperature range of 25 °C to 1000 °C, the TGA curve exhibits two distinct weight loss steps

and the DTGA curve presents five corresponding exothermic peaks and one endothermic peak. The first weight loss step (19.42%) was the range of 25–450 °C, which was accompanied by one exothermic sharp peak around 35 °C and another small exothermic peak located at 175 °C in the DSC curve. These peaks could be attributed to the combustion of nitrates and the remaining organic substances, respectively. Moreover, the small exothermic peak at nearly 450 °C refers to the oxidation of carbon from glycine by oxygen in the air that forms carbon dioxide and releases heat [14]. The second weight loss step (66.91%) in the range of 500–1000 °C with released heat due to lattice relaxation and the cations reordering between tetrahedral and octahedral sites. Beside the large exothermic peak, on the heating curve an endothermic peak can be also remarked [15]. Small endothermic sharp peak around 600 °C is associated with complete conversion of the reacting oxides yielding the corresponding ferrite. Moreover, two exothermic broad peaks in the range of 675–1000 °C refer to the distorted structure of the ferrite, implying the presence of cation redistribution in Zn and Co substituted manganese ferrite within this temperature range.

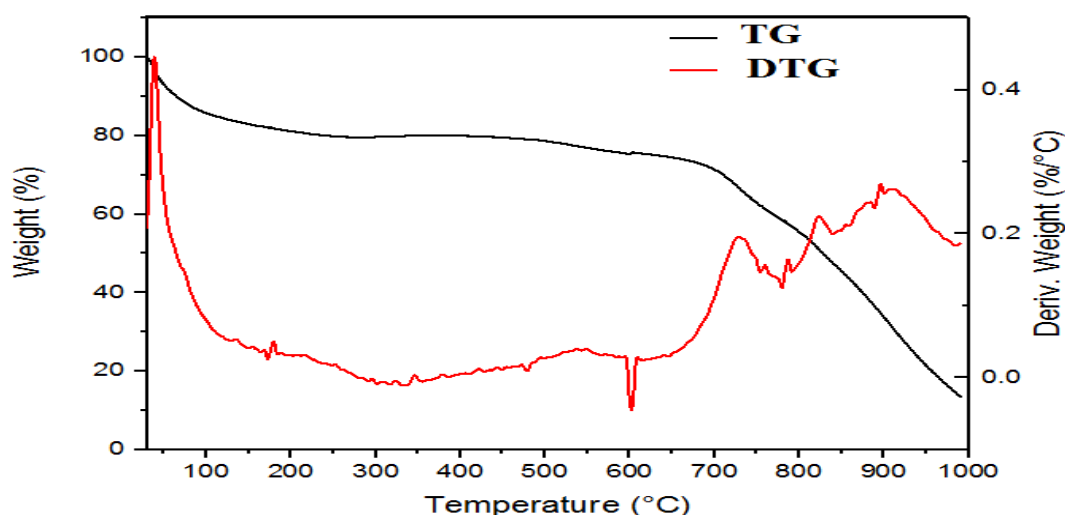


Fig. 1. TG and DTG pattern of the uncalcined powders.

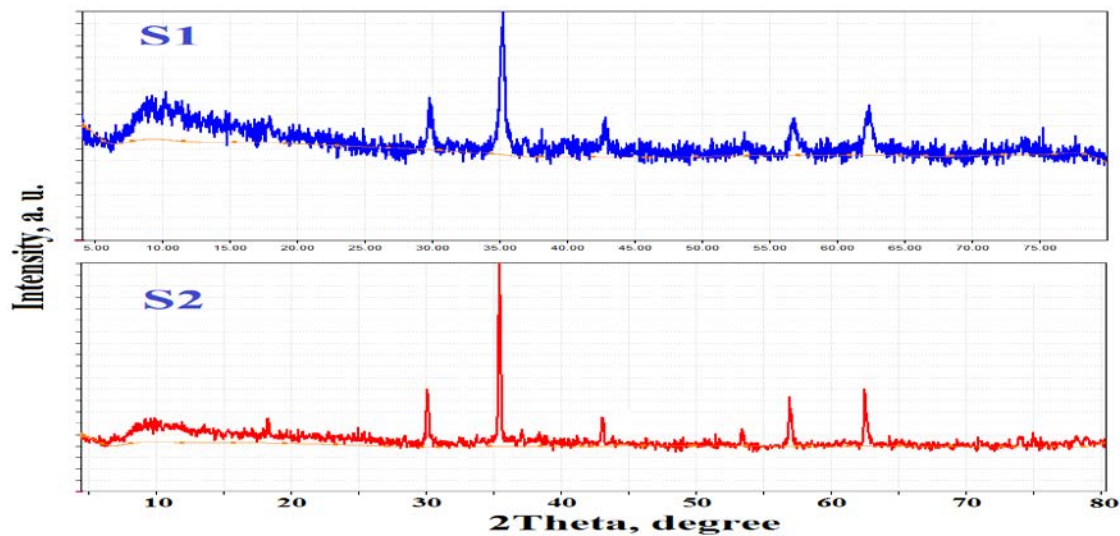
### 3.2. Structural analysis

In order to determine the purity phase and the structural characteristics of the investigated solids, using of XRD technique was very important for these aims. Fig. 2 shows XRD of the synthesized solid (S1 and S2) calcined at 600 °C and 800 °C. Various diffraction peaks were observed in XRD pattern of the S1 samples at  $2\theta = 18.00^\circ, 29.76^\circ, 34.95^\circ, 36.80^\circ, 42.54^\circ, 52.82^\circ, 56.53^\circ, 62.18^\circ, 73.57^\circ$  and  $75.05^\circ$ , these diffraction peaks associated with the corresponding planes (111), (220), (311), (222), (400), (422), (511), (440), (620) and (533) of a cubic spinel structure with the space group  $Fd\bar{3}m$ . It was found that an increase in calcination temperature resulted in a shift in the position of the previous peaks as shown in the case of the S2 sample. Investigation of this figure revealed that: (i) Increasing the heat treatment from 600 °C to 800 °C brought an increase in different peaks height with subsequent increase in their sharpness. (ii) Any second phase is not present in the final product. This confirms that the preparation method followed by heating at different temperatures is good for production mixed ferrite in a single phase with high purity. (iii) the crystallite size of the produced solid increases as the calcination temperature increases from 600 °C to 800 °C as shown in Table I. This behavior could be attributed to agglomeration and/or grain growth of the particles studied.

**Tab. I** Lattice parameters of the S1 and S2 samples.

Parameters	S1	S2
d, nm	23	67
a, nm	0.8452	0.8477
V, nm <sup>3</sup>	0.6038	0.6092
D <sub>x</sub> , g/cm <sup>3</sup>	5.1542	5.1085
L <sub>A</sub> , nm	0.3660	0.3671
L <sub>B</sub> , nm	0.2987	0.2996
A-O, nm	0.1932	0.1938
B-O, nm	0.2181	0.2187
r <sub>A</sub> , nm	0.0612	0.0618
r <sub>B</sub> , nm	0.0861	0.0867
δ, Lines/nm <sup>2</sup>	1.890 x 10 <sup>-3</sup>	0.222 x 10 <sup>-3</sup>

In order to clarify the crystalline nature of the prepared ferrites, it is necessary to calculate the various parameters related to the structural properties that listed in Table I. Some of parameters were the lattice constant (a), unit cell volume (V), X-ray density (D<sub>x</sub>), the distance between the magnetic ions (L<sub>A</sub> and L<sub>B</sub>), ionic radii (r<sub>A</sub>, r<sub>B</sub>), dislocation density (δ), and bond lengths (A-O and B-O) on tetrahedral (A) sites and octahedral (B) sites. A careful analysis of the results of this table found the following: (i) Increasing the calcination temperature resulted in an increase in values of a, V, L<sub>A</sub>, L<sub>B</sub>, r<sub>A</sub>, r<sub>B</sub>, A-O and B-O as shown in the S2 sample. An opposite finding was observed in the D<sub>x</sub> and δ values. (ii) The values of A-O and r<sub>A</sub> are smaller than that of r<sub>B</sub> and B-O. Opposite behavior was observed in the values L<sub>A</sub> relative to that of L<sub>B</sub>. Due to the heat treatment, the maximum increase in both values of A-O and r<sub>A</sub> was found to be 0.31% and 0.98%, respectively. Whereas, the maximum increase in both values of B-O and r<sub>B</sub> was found to be 0.28% and 0.70%, respectively. In addition, the maximum increase in both values of L<sub>A</sub> and L<sub>B</sub> was the same increase which was found to be 0.30%. (iii) The structural parameters based findings suggested that the effect of heat treatment of the investigated ferrite was more pronounced at A-site indicating cation redistribution in Zn substituted cobalt -manganese ferrites.

**Fig. 2.** XRD patterns of S1 and S2 samples.

The FTIR spectra of the S1 and S2 samples were illustrated in Fig. 3. These spectra exhibit two main absorption bands,  $\nu_1 \sim 600 \text{ cm}^{-1}$  and  $\nu_2 \sim 400 \text{ cm}^{-1}$  which may be attributed to the A and B sites in the spinel lattice, respectively. In this study the FTIR spectra of the analyzed ferrites containing Zn, Co, Mn and Fe cations show two main absorption bands: the one in the wave number range of  $\sim 698 - 475 \text{ cm}^{-1}$  is assigned to the stretching vibrations,  $\nu_1$ , of the tetrahedral complexes and the other low-frequency band at  $\sim 432- 404 \text{ cm}^{-1}$  is assigned to the stretching vibrations,  $\nu_2$ , of the octahedral complexes with oxygen [5]. Furthermore, the splitting of these two main IR absorption bands into several sub-bands has been observed in the previous figure. However, the same functional groups of the S1 and S2 sample were observed with change in their intensities and frequencies. A progressive change occurred at the tetrahedral site from  $475 \text{ cm}^{-1}$  to  $467 \text{ cm}^{-1}$  due to migration of  $\text{Fe}^{3+}$  ions to the octahedral site depending on thermal treatment. The splitting of the absorption band near  $\nu_2 \sim 400 \text{ cm}^{-1}$  has been clearly observed. The splitting of octahedral (B-site) absorption band is due to the presence of three kinds of cations at the B-site:  $\text{Co}^{2+}$ ,  $\text{Mn}^{3+}$  and  $\text{Fe}^{3+}$  [5-7]. On the other hand, the splitting of the absorption band near  $\nu_1 \sim 600 \text{ cm}^{-1}$  could be attributed to the presence of  $\text{Zn}^{2+}$ ,  $\text{Mn}^{2+}$  and  $\text{Fe}^{3+}$  ions [5]. Furthermore, three bands were observed at  $1330-1307$ ,  $1148-1144$ , and  $991-985 \text{ cm}^{-1}$  due to the stretching vibrations of a hydroxyl carbon (C-O-H) [16].

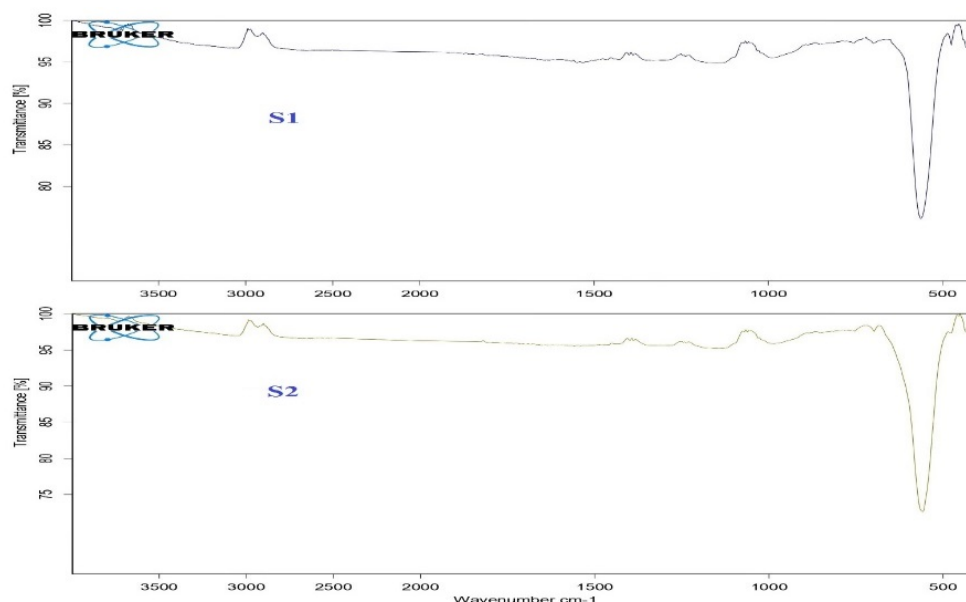


**Fig. 3.** Fourier-transform infrared (FTIR) spectrum of S1 and S2 samples.

### 3.4. SEM and EDS analyses

Using SEM technique was enabled to determine the surface morphology of the S1 sample. SEM image is presented in Fig. 4. This figure shows porous material with different voids and pores. This material has a sponge and fragile shape. Determination of the elemental constituents of the S1 sample was achieved by using EDS measurement. The table attached EDS pattern displays that the S1 consisted entirely of Zn, Co, Mn, Fe and C elements with different ratios. From this table the order of element weights was as follows:  $\text{Fe} > \text{Mn} \geq \text{Co} > \text{Zn}$ . This trend is consistent with the proportions used in the preparation process.

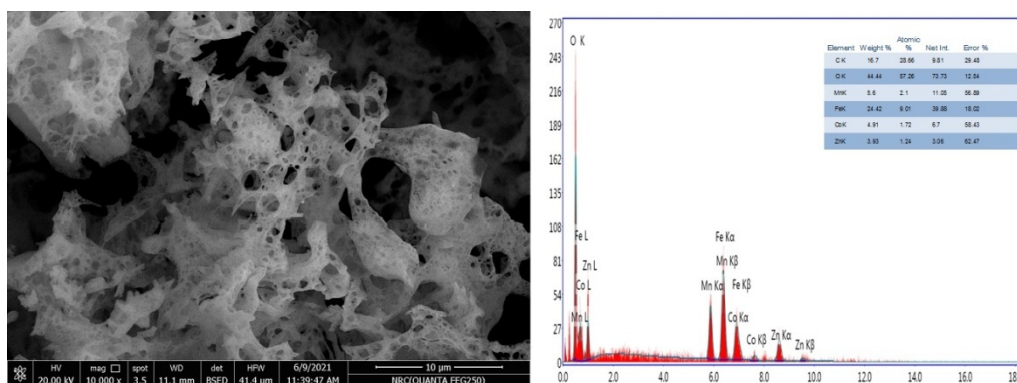


Fig. 4. SEM image and EDS pattern of the S1 sample.

### 3.5. TEM measurements

A deeper study of the morphological properties can be occurred by using TEM technique. Fig. 5 represents a contains TEM image of the S2 sample. This figure shows clear adhesion between the different particles with full clarity of their boundaries. In addition, some agglomerations were observed depending on rise in the calcination temperature. Despite the high heat treatment temperature, the particles of the resulting material are still in the nanometer range. It was of great importance to determine the size distribution of the particles, which was evident in Fig. 5c. Through this figure, it is clear that the particles treated thermally at 800 °C are large in size, as it was found that the average size of the grains of these particles was at 80 nm. In addition, the prepared material retains many cavities between the collected particles, which gives it the porous property as shown in Fig. 5a. In addition, Fig. 5b shows the selected area electron diffraction (SAED) image consisted entirely of various rings indicating the presence of polycrystalline particles. However, the investigated sample has a non-uniform intensity distribution along the resulting rings despite crystallinity sufficient for generating smooth rings. In addition, the appearance of many bright spots with different sizes and illumination confirms that this material contains elements of different nature, which were identified through EDS analysis.

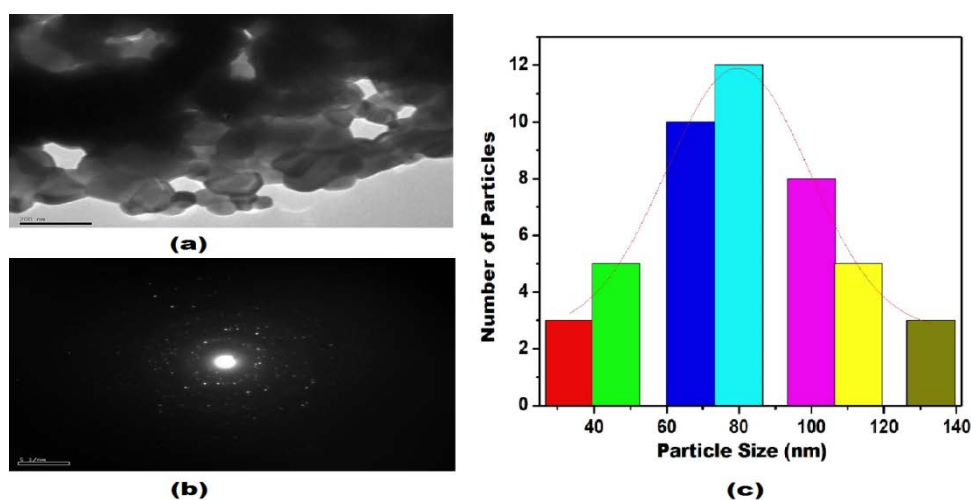
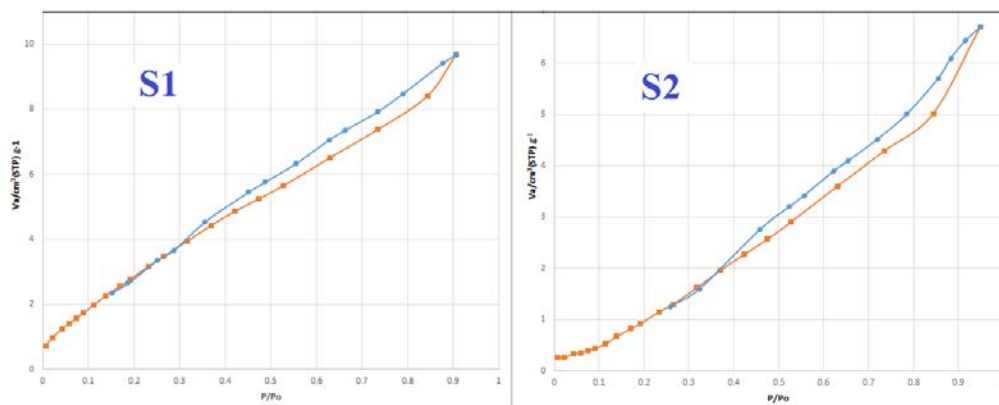


Fig. 5. (a) transmission electron micrograph (TEM) image, (b) selected-area electron diffraction (SAED) pattern and (c) particle size distribution of S2 sample.

### 3.6. Surface characteristics

The porosity of the materials was confirmed by determining their surface properties. Through  $N_2$  adsorption/desorption on the surface of the prepared materials at 77 K, we were able to obtain different isotherms, followed by determining the different surface properties. These isotherms were constructed in Fig. 6, which were found to belong to II- type with the presence of hysteresis loop of H3- type.



**Fig. 6.**  $N_2$ -adsorption/desorption isotherms of the S1 and S2 samples.

Table II depicts the results of surface properties of the investigated ferrites. Increasing the heat treatment led to a clear decrease in all surface properties.

**Tab. II** Surface properties of the S1 and S2 samples.

Samples	$S_{BET}$ ( $m^2/g$ )	$V_p$ ( $cm^3/g$ )	$\bar{r}$ (nm)	$V_m$ (nm)	C-constant
S1	14.562	0.0153	4.197	3.346	8.761
S2	8.824	0.0088	3.999	2.0274	2.473

Increasing the temperature from 600 to 800 °C brought a decrease in the surface area of the prepared ferrites by 39%. While the decrease in the total pore volume was 42.5%. This severe deficiency was confirmed by the decrease in the volume of the monolayer adsorbed nitrogen molecules on the ferrite surface, in which the percentage of decrease was 11.8%. All this decrease in all the above was associated with a decrease in the mean pore radius, which was 4.7%. These results were consistent with the shift in the position of the only peak observed in Fig. 7.

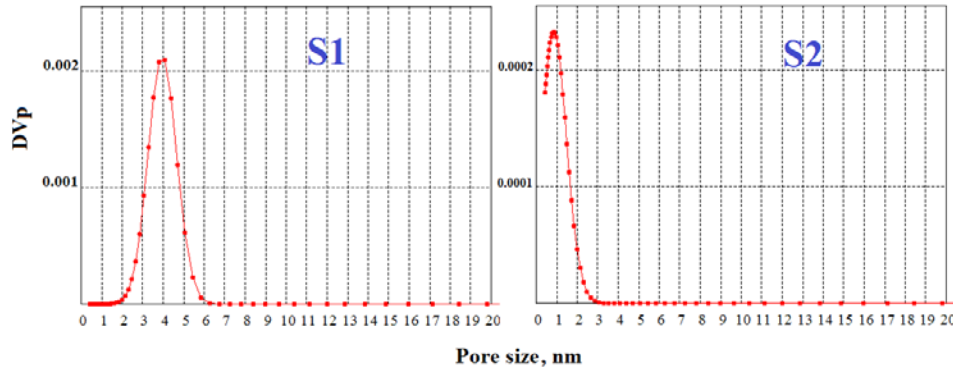


Fig. 7. Pore size distribution patterns of the S1 and S2 samples.

### 3.7. Magnetization of the manufactured ferrites

The different magnetic properties of the as-prepared ferrites were investigated by measuring the magnetic hysteresis loop at room temperature and applied magnetic field in the range of  $\pm 20$  kG with illustration of M-H curves as shown in Fig. 8. The magnetic properties included many factors that strongly indicate the magnetic nature of the materials, which are strongly affected by the structural, morphological, and surface properties of these materials.

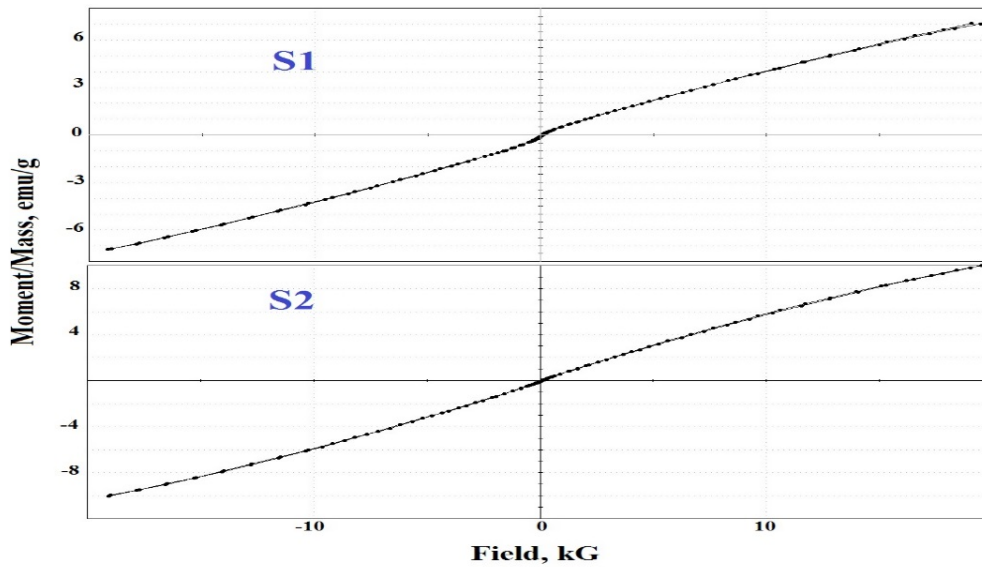


Fig. 8. M–H curves at room temperature for S1 and S2 samples.

In this context, we find that the results obtained in Table III indicate the following: (i) increasing the roasting temperature of the prepared ferrites from 600 to 800 °C led to an increase in the saturation magnetization ( $M_s$ ) of these ferrites with subsequent a decrease in the values of the remanent magnetization ( $M_r$ ), squareness ( $M_r/M_s$ ) and coercive field ( $H_c$ ). (ii) This treatment resulted in an increase in the values of an initial permeability ( $\mu_i$ ) and magnetic moment ( $\mu_m$ ) per unit formula in Bohr magnetron of the investigated ferrites. On other hand, anisotropy constant ( $K_a$ ) of the ferrites studied decreases by increasing the calcination temperature from 600 to 800 °C.

**Tab. III** The magnetic properties of the S1 and S2 samples.

Samples	$M_s$ (emu/g)	$M_r$ (emu/g)	$M_r/M_s$ (emu/g)	$H_c$ (Oe)	$\mu_m$	$\mu_i$	$K_a$ (erg/cm <sup>3</sup> )
S1	7.140	0.0258	0.0036	23.245	0.2995	6.7821	127.885
S2	10.014	0.0111	0.0011	11.871	0.4200	44.5405	123.829

#### 4. Discussion

The morphological structure of the investigated ferrite strongly depended on the heat treatment. Based on SEM analysis of the S1 specimen, it is found that the ferrite calcined at 600 °C showed a spongy structure due to the volatilization of different gases with combustion of both glycine and nitrates. In addition, observation of high dispersion, relatively regular spherical-like shape, and moderate particle size, which brought an increase in the surface area and total pore volume. By the observation of TEM image of the S2 specimen, it is important to point out that the S1 sample did not sinter as the S2 sample, but had many discernible tiny pores. The particles of the S2 sample were found to be of moderate size and irregular shape due to grain growth and the change in the cation distribution.

The surface properties are a fundamental and important for the interpretation and connection of most material characteristics. We can take the surface properties as a mirror to express their structural and morphological properties, which will in turn affect many of the applied properties of these materials such as magnetic features. In our current study, it was found that changing the heat treatment by increasing the calcination temperature led to a clear change in all structural properties. Increasing the temperature from 600 to 800 °C led to a clear increase in the degree of crystallization and the lattice constant. The change did not stop at this point, but also caused other changes in the cation distribution, size and shape of the particles. Indeed, the studied samples included two processes of agglomeration and grain growth as a result of increasing the calcination temperature. However, we see that the process of growth is predominant and most influential in occurring of the previous changes, in addition to the noticeable change in the cation distribution.

By careful examination of surface properties based on the figures (Figs. 6 and 7) and the results present in Table II, it was found that: (i) The isotherms pointed to the disordered, lamellar micro/mesoporous structure of the S1 and S2 samples. Obviously, the adsorption capacity of the S1 sample was greater than that of the S2 sample. The S1 sample had values of both the surface area and pore volume greater than those for the S2 sample which was consistent with the SEM and TEM observations. In other words, the sequences of surface area and pore volume were completely consistent with the adsorption capacity of the prepared sample. (ii) The pore size distribution pattern shows that increasing of calcination temperature from 600 to 800 °C resulted in shift of the major peak of the one model from 4 nm to 0.9 nm. This could be attributed to the obvious decrease in the mean pore radius, and the transformation of most mesopores into micropores as a result of grain growth of particles as shown in TEM image. One cannot ignore coexistence of both micro- and mesopores, but in different proportions that differ according to the history of the prepared materials. These findings confirm that the pore size and particle size played a pivotal role in the material's adsorption capacity as shown in the  $V_m$  values. Thus, it was necessary to determine the surface properties of the prepared materials due to the importance of clarifying the surface properties in explaining many their properties, including catalytic, electrical and magnetic properties. Where, the magnetic properties are related to the surface properties by a common factor among them, which depends on the grain size which is associated with grain boundaries.

The saturation magnetization of Zn substituted Co-Mn ferrite increases with increasing calcination temperature from 600 to 800 °C. This means that the heat treatment has

a significant impact on the different contents of the investigated ferrite, then on its net magnetism. This could be explained by the cation redistribution and the super exchange of metal ions in the tetrahedral (A-) and octahedral (B-) sites in the spinel ferrite lattice. Through the first look the hysteresis loops, it is found that these loops has the S-shape, a clear indication that the prepared ferrites have the ferromagnetic behavior [16]. When we carefully examine the results recorded in Table III, it turns out the following: (i) the magnetism of the prepared ferrites increases with the increase in the calcination temperature as a result of the increase in the size of the particles depends on the increase in the lattice constant. In other words, the grain growth due to an increase in the calcination temperature of the ferrite particles resulted in an increase in their lattice constant with subsequent increase in their size of particles. In addition, increasing the heat treatment from 600 to 800 °C may be enhanced the migration of some ferric ions from A-site to B-site and transformation of ferrous ions to ferric ions at B-site with subsequent an increase in the net magnetic moment. Indeed, this treatment brought about an increase in the value of  $\mu_m$  as shown in Table III. In the crystal structure of Zn substituted Co- Mn ferrite,  $Zn^{2+}$  occupies A-sites,  $Co^{2+}$ ,  $Fe^{2+}$  and  $Mn^{3+}$  ions have a tendency to enter into B-sites, and  $Fe^{3+}$  and  $Mn^{2+}$  occupy either A-sites or B-sites randomly [17]. Increasing of the calcination of brought about transformation of  $Fe^{2+}$  to  $Fe^{3+}$  at B-site with migration of some  $Fe^{3+}$  from A- site to B- site yielding an increase in different lattice parameters as observed in Table I. (ii) The investigated ferrites have uniaxial anisotropy rather than cubic anisotropy because the squareness ratio ( $M_r/M_s$ ) is less than "0.5". In addition, the small squareness values referred to the surface spin disorder effects due to the canted spin on the surface of nanoparticles. Hence, the lower value of this ratio strongly pushes the studied ferrites towards their use in high-frequency applications [18-20]. (iii) increasing the calcination temperature brought about a decrease in the coercivity of Zn substituted Co- Mn ferrite due to a decrease in the magnetic anisotropic constant. Narrow hysteresis loops indicate low values of coercivity of the as-prepared samples with subsequent demagnetization for electromagnetic applications [21-27].

#### 4. Conclusion

Glycine based auto combustion route followed by heating at 600 °C and 800 °C for 2h resulted in formation  $Zn_{0.2}Co_{0.4}Mn_{0.4}Fe_2O_4$  nanoparticles. This treatment resulted in different changes in various features of the as-prepared ferrite as follows:

- 1- Increasing the calcination temperature led to an increase in a lattice constant of  $Zn_{0.2}Co_{0.4}Mn_{0.4}Fe_2O_4$  nanoparticles from 0.8452 nm to 0.8477 nm with subsequent increase in the crystallite size from 23 nm to 67nm.
- 2- The heat treatment of the investigated ferrite brought shift in the intensity and position of characteristic vibrational modes that located around  $600\text{ cm}^{-1}$  and  $400\text{ cm}^{-1}$ .
- 3- Based on the SEM analysis, porous, fluffy, foamy and fragile material was observed. Moreover, EDX analysis confirms that the resulting material consisted entirely of Zn, Co, Mn, Fe and O elements.
- 4- Various surface characteristics of the as-manufactured material were changed by increasing the calcination temperature. The surface area, total pore volume and mean pore radius of the obtained ferrite were decreased by increasing the heat treatment from 600 °C and 800 °C.
- 5- Increasing the calcination temperature from 600 °C and 800 °C brought an increase in the magnetization of the as-synthesized material due to an increase in particle size with subsequent change in cation distribution.
- 6- Finally, the investigated method is suitable for preparation of different transition metal substituted mixed ferrite nanoparticles for various applications.

## Acknowledgments

The author acknowledges the financial support of this work by National Research Centre(NRC), Cairo, Dokki, Egypt, via the project No.12020223.

## 5. References

1. N. M. Deraz, A. Alarifi, "Controlled Synthesis, Physicochemical and Magnetic Properties of Nano-Crystalline Mn Ferrite System", *Int. J. Electrochem. Sci.*, 7 (2012) 5534 – 5543.
2. M. A. Ahmed, N. Okasha, M. M. El-Sayed, "Enhancement of the Physical Properties of Rare-Earth-Substituted Mn–Zn Ferrites Prepared by Flash Method", *Ceram. Int.*, 33 (2007) 49-58.
3. Z. K. Heiba, M. B. Mohamed, A. M. Wahba, Arda, L. Magnetic, "Structural Properties of Nano-Crystalline Cobalt Substituted Magnesium-Manganese Ferrite", *J. Supercond. Nov. Magn.*, 28 (2015) 2517–25248.
4. K. Janghorban, H. Shokrollahi, "Influence of V<sub>2</sub>O<sub>5</sub> Addition on the Grain Growth and Magnetic Properties of Mn-Zn High Permeability Ferrites", *J. Magn. Magn. Mater.*, 308 (2007) 238–242
5. N. M. Deraz, A. Alarifi, Preparation and Characterization of Nano-Magnetic Mn<sub>0.5</sub>Zn<sub>0.5</sub>Fe<sub>2</sub>O<sub>4</sub> System", *Int. J. Electrochem. Sci.*, *Int. J. Electrochem. Sci.*, 7 (2012) 5828 – 5836.
6. R. Arulmurugan, B. Jeyadevan, G. Vaidyanathan, S. Sendhilnathan, "Effect of Zinc Substitution on Co-Zn and Mn-Zn Ferrite Nano-Particles Prepared by co-precipitation", *J. Magn. Magn. Mater.*, 288 (2005) 470–477
7. N. M. Deraz, A. Alarifi, "Structural, Morphological and Magnetic Properties of Nano-Crystalline Zinc Substituted Cobalt Ferrite System", *J. Analyt. Appl. Pyrolysis*, 94 (2012) 41–47.
8. N. M. Deraz, O. H. Abd-Elkader, "Synthesis and Characterization of FeO/Ni<sub>0.5</sub>Mn<sub>0.5</sub>Fe<sub>2</sub>O<sub>4</sub> Nano- Composite", *Asian J. Chem.*, 26 (2014) 2141- 2146.
9. N. M. Deraz, O. H. Abd-Elkader, "Processing and Characterization of Nano-Magnetic Co<sub>0.5</sub>Ni<sub>0.5</sub>Fe<sub>2</sub>O<sub>4</sub> System", *J. Ind. Eng. Chem.*, 20 (2014) 3251-3255.
10. N. M. Deraz, O. H. Abd-Elkader, "Production and Characterization of Nano-Magnetic Ni<sub>0.5</sub>Zn<sub>0.5</sub>Fe<sub>2</sub>O<sub>4</sub> Spinel Solid Solution", *J. Analyt. Appl. Pyrolysis*, 106 (2014) 171-176.
11. G. Mathubala, A. Manikandan, S. Arul Antony, P. Ramar, "Photocatalytic Degradation of Methylene Blue Dye and Magneto-optical Studies of Magnetically Recyclable Spinel Ni<sub>x</sub>Mn<sub>1-x</sub>Fe<sub>2</sub>O<sub>4</sub> (x = 0.0-1.0) Nanoparticles", *J. Mol. Struct.*, 113 (2016) 79–87.
12. B. Sudakshina, M. V. Suneesh, B. Arun, K. Chandrasekhar, M. Vasundhara, "Effects of Cr, Co, Ni Substitution at Mn-site on Structural, Magnetic Properties and Critical Behaviour in Nd<sub>0.67</sub>Ba<sub>0.33</sub>MnO<sub>3</sub> Mixed-Valent Manganite", *J. Magn. Magn. Mater.*, 548 (2022) 168980.
13. N. M. Deraz, A. M. Abdel-karim, "Simple Synthesis, Structural and Magnetic Properties of Zn<sub>0.2</sub>Co<sub>0.4</sub>Mn<sub>0.4</sub>Fe<sub>2</sub>O<sub>4</sub> System" *Nanosci. Nanotechnol. Open Access*, 1 (2022) 1003.
14. S. A. Saafan, N. M. Abo-Aita, E. H. El Ghazzawy, "Preparation and Structural Investigation of Polyethylene Glycol (PEG) / Nano-Ferrite Composites", *Egypt J. Solids*, 43 (2021) 174-191.

15. T.F. Marinca, I. Chicinas, O. Isnard, V. Pop, F. Popa, "Synthesis, Structural and Magnetic Characterization of Nanocrystalline Nickel Ferrite—NiFe<sub>2</sub>O<sub>4</sub> obtained by Reactive Milling, J. Alloys Compd., 509 (2011) 7931– 7936.
16. G. M. Al-Senani, F. F. Al-Fawzan, R. S. Almufarij, O. H. Abd-Elkader, N. M. Deraz, "Biosynthesis, Physicochemical and Magnetic Properties of Inverse Spinel Nickel Ferrite System", Crystals, 12(2022)1542.
17. H. Anwar, A. Maqsood, "Comparison of Structural and Electrical Properties of Co<sup>2+</sup> Doped Mn-Zn Soft Nano Ferrites Prepared via co-precipitation and Hydrothermal Methods", Mater. Res. Bull., 49 (2014) 426–433.
18. P. A. Rao, K. S. Rao, T. P. Raju, G. Kapusetti, M. Choppadandi, M. C. Varma, K. H. Rao, "A systematic Study of Cobalt-Zinc Ferrite Nanoparticles for Self-Regulated Magnetic Hyperthermia", J. Alloys Compd., 794 (2019) 60–67.
19. Q. A. Pankhurst, R. J. Pollard, "Origin of the Spin-Canting Anomaly in Small Ferrimagnetic Particles", Phys. Rev. Lett., 67 (1991) 248-250.
20. J. Joseph, R. B. Tangsali, V. P. M. Pillai, R. J. Choudhary, D. M. Phase, V. Ganeshan, "Structure and Magnetic Properties of Highly Textured Nanocrystalline Mn-Zn Ferrite Thin Film", Phys. B: Condens. Matter., 456 (2015) 293–297.
21. Q. Y. Zhang, P. Zheng, L. Zheng, J. Zhou, H. Qin, "Effect of Co-Substitution on the Structure and Magnetic Properties of Mn Zn Power Ferrite", J. Electroceram., 32 (2014) 230–233.
22. H. Anwar, A. Maqsood, I. H. Gul, "Effect of Synthesis on Structural and Magnetic Properties of Cobalt Doped Mn-Zn Nano Ferrites", J. Alloys Compd., 626 (2015) 410–414
23. A. Lassoued, M. Ben hassine, F. Karolak, B. Dkhil, S. Ammar, A. Gadri, "Synthesis and Magnetic Characterization of Spinel Ferrites MFe<sub>2</sub>O<sub>4</sub> (M = Ni, Co, Zn and Cu) via Chemical Co-precipitation Method" J. Mater. Sci. Mater. Electron., 28 (2017) 18857–18864.
24. B. W. Wang, C. C. Gao, H. B. Zhao, C. G. Zheng, "Preparation of CoFe<sub>2</sub>O<sub>4</sub> Nanocrystallite by Sol-Gel Combustion Synthesis and Evaluation of its Reaction Performance", Adv. Mater. Res., 341–342(2011)63–67.
25. A. Jr. Franco, H. V. S. Pessoni, F.O. Neto, "Enhanced High Temperature Magnetic Properties of ZnO-CoFe<sub>2</sub>O<sub>4</sub> Ceramic Composite", J. Alloys Compd., 680 (2016) 198–205.
26. S. K. Jesudoss., J. J. Judith Vijaya, L. J. John Kennedy, P. I. Rajan, H. A. Al-Lohedan, R. J. Jothi Ramalingam, K. Kaviyarasu, M. Bououdina, "Studies on the Efficient Dual Performance of Mn<sub>1-x</sub>Ni<sub>x</sub>Fe<sub>2</sub>O<sub>4</sub> Spinel Nanoparticles in Photodegradation and Antibacterial Activity", J. Photochem. Photobiol. B, 165 (2016) 121–132.
27. N. M. Deraz, "Facile and eco-friendly route for green synthesis of magnesium ferrite nano particles", Sci. Sinter., 52 (2020) 53-65.

---

**Сажетак:** Метода самосагоревања уз помоћ глицина резултирала је производњом кобалт-манган ферита супституисаног елементом цинка (Zn). Синтетисани Co- Mn ферит је подвргнут топлотној обради на 600 °C и 800 °C током 2 сата. Проучавани су ефекти термичке обраде на структурна, морфолошка, површинска и магнетна својства ZnCoMn ферита. Ова својства су окарактерисана коришћењем различитих техника укључујући ТГА-ДТГА, ФТИР, рендген, СЕМ, ТЕМ и ВСМ. Резултати су показали да је коришћени метод припреме довео до формирања нанокристалних честица Zn<sub>0,2</sub>Co<sub>0,4</sub>Mn<sub>0,4</sub>Fe<sub>2</sub>O<sub>4</sub> са кубичном структуром типа спинела. Кристаличност овог ферита се повећава како се повећава температура калцинације. Међутим, начин

---

припреме резултирао је стварањем сунђерастог, пахуљастог, пенастог и ломљивог материјала са структуром кубног типа са агломератима. Повећање температуре калцинације са 600 °C на 800 °C довело је до смањења површине (39,4 %) синтетисаног ферита. Овај третман изазива повећање магнетизације (40,3 %) ферита. Разматрана је термичка обрада која је довела до различитих промена у различитим својствима произведеног ферита.

**Кључне речи:** XRD, FTIR, SEM, ZnCoMn ферит, магнетизација.

---

© 2023 Authors. Published by association for ETRAN Society. This article is an open access article distributed under the terms and conditions of the Creative Commons — Attribution 4.0 International license (<https://creativecommons.org/licenses/by/4.0/>).

